Atmospheric Research 98 (2010) 363–367

Contents lists available at ScienceDirect

Atmospheric Research

journal homepage: www.elsevier.com/locate/atmos

Measuring the influence of aerosols and albedo on sky polarization

A. Kreuter [a,b,*], C. Emde [c], M. Blumthaler [a]

[a] Division for Biomedical Physics, Department of Physiology and Medical Physics, Innsbruck Medical University, Innsbruck, Austria
[b] Department of Physics, University of California, Berkeley, USA
[c] Meteorological Institute, Ludwig-Maximilians-University, Munich, Germany

ARTICLE INFO

Article history:
Received 7 April 2010
Received in revised form 22 June 2010
Accepted 19 July 2010

Keywords:
Polarized sky radiance
Aerosols
AOD
Albedo
All-sky camera

ABSTRACT

All-sky distributions of the polarized radiance are measured using an automated fish-eye camera system with a rotating polarizer. For a large range of aerosol and surface albedo situations, the influence on the degree of polarization and sky radiance is investigated. The range of aerosol optical depth and albedo is 0.05–0.5 and 0.1–0.75, respectively. For this range of parameters, a reduction of the degree of polarization from about 0.7 to 0.4 was observed. The analysis is done for 90° scattering angle in the principal plane under clear sky conditions for a broadband channel of 450 ± 25 nm and solar zenith angles between 55° and 60°. Radiative transfer calculations considering three different aerosol mixtures are performed and and agree with the measurements within the statistical error.

1. Introduction

Atmospheric molecules scatter the solar radiation producing a blue sky of diffuse polarized radiance (Chandrasekhar and Elbert, 1951). Additional scattering due to aerosols and back reflections from the ground (and clouds) tend to increase the radiance and reduce the degree of polarization. While the ground albedo is relatively constant over large areas and long timescales, aerosol optical properties vary strongly in space and time and remain a pivotal uncertainty in the planet's radiation energy budget (IPCC report, 2007). In space and ground-based passive remote sensing, sky radiance is the key observable to access optical aerosol parameters like single scattering albedo (SSA) and asymmetry factor, the extrinsic parameters determining the radiative forcing. Often, the SSA is also derived by the "shadow band technique" measuring global and diffuse irradiance. The spectral aerosol column density is commonly determined by extinction measurements of the direct sun irradiance (sun photometers) and is described by the aerosol optical depth (AOD).

The ground-based global aerosol robotic network (AERONET) combines sky radiance and direct sun measurements using a sky-scanning radiometer to retrieve optical aerosol parameters (Holben et al., 1998; Dubovik and King, 2000). Measuring the radiance's full polarization state adds valuable information as it is sensitive to aerosol microphysical properties and improves retrieval (Vermeulen et al., 2000; Boesche et al., 2006; Li et al., 2006, 2009).

Polarized radiance observations are included in modern satellites, e.g. the POLDER instrument which flew on two missions in the past (Deuze et al., 2001), and the APS instrument scheduled to fly on the GLORY mission (Mishchenko et al., 2007).

The theoretical dependence of the degree of polarization on AOD and albedo was first quantified by Coulson et al. (1960). In specific case studies, the degree of polarization was correlated also experimentally with AOD measurements (Masuda et al., 1999; Shukurov and Shukurov, 2006).

Here, data of polarized sky radiance distribution maps sampled from a three year period in Innsbruck and Vienna, Austria, are shown, exploring the dependence on a large range of aerosol loads and albedos. Data also include measurements in a high albedo arctic environment on Svalbard, Norway.

* Corresponding author. Division for Biomedical Physics, Department of Physiology and Medical Physics, Innsbruck Medical University, Innsbruck, Austria.
E-mail address: axel.kreuter@uibk.ac.at (A. Kreuter).

0169-8095
doi:10.1016/j.atmosres.2010.07.010

2. Method

Using ground-based all-sky cameras, hemispherical maps of the polarized radiance have been presented (Liu and Voss, 1997; Gál et al., 2001; North and Duggin, 1997; Kreuter et al., 2009). The all-sky camera system used here consists of a commercial compact digital camera with a fish-eye objective (field-of-view (FOV) ≈ 180°) and a stepping motor controlled linear polarizing filter, situated between the objective and the camera. The system is mounted in a weather-proof housing with a glass dome and connected via ethernet cable to a PC for external automated control. The images are transmitted in *jpg* format and have an intensity resolution of 8 bit for three color channels (RGB) and a spatial resolution of 1536 × 2048 pixels. The whole process of acquiring the set of 4 images, rotating the polarizer and transmitting the data takes less than a minute. A shadow mechanism is omitted here for simplifying the system with less moving parts and less obscured sky. Problems include the area around the direct sun (aureole) which is difficult for image processing, and reflections in the lens system perturbing the image at certain zenith angles.

Each pixel can be considered a set of 3 independent broadband detectors. Since each pixel is illuminated by a radiant power from a certain solid angle and integrated over the spectral responsivity the measured radiometric quantity is radiance. The radiance R at each pixel is a non-linear function of the stored pixel counts C, $R = k \cdot f(C)$, where k is a calibration constant for radiance in absolute units. Since no absolute calibration was performed explicitly, a relative polarized radiance is obtained for each pixel after applying the non-linear response function $f(C)$. A detailed characterization of the system and image processing has been given by Kreuter et al. (2009).

The generalized polarization state of light is commonly described by the Stokes vector (see e.g. Coulson, 1988). Its four components (I, Q, U, V) are real-valued observables, defined via linear combinations of orthogonal complex field amplitudes (and their conjugates). In the terms used here, the Stokes vector is given by the following:

$$\begin{bmatrix} I \\ Q \\ U \end{bmatrix} = \begin{bmatrix} R_0 + R_{90} \\ R_0 - R_{90} \\ R_{45} - R_{135} \end{bmatrix} \quad (1)$$

where R_α denote the measured radiances at relative polarizer angles α. The fourth component V describing circular polarization is assumed zero for the sky radiance. Geometrically, Q/I and U/I are the two orthogonal components in the equator plane of the Poincaré sphere, while I is the total (unpolarized) absolute radiance. Conversion to spherical coordinates, yields the degree of linear polarization Π:

$$\Pi = \frac{\sqrt{Q^2 + U^2}}{I} \quad (2)$$

A set of four relative polarized radiance maps at polarizer angles of 0°, 45°, 90° and 135° is stored and, after applying Eq. (1) at each pixel, hemispherical distribution maps of all Stokes components are computed. Note that calibration is not required for determining Π since the calibration constant k cancels in Eq. (2).

In this study we restrict ourselves to Π and I of the blue channel of the camera with a center wavelength of 450 nm and a full width at half maximum (FWHM) of 50 nm.

The method has been validated against a well-characterized spectroradiometer with a scanning polarized radiance optics (Blumthaler et al., 2008). More than 20° away from overexposed pixels around the sun the agreement of Π was within 0.03, which agrees with the statistical error inferred from consecutive measurements under constant conditions. In the same way, the statistical error of I is inferred to be 8%.

The AOD measurements are performed with a co-located precision-filter-radiometer (PFR) sunphotometer with 4 channels at wavelengths of 368 nm, 412 nm, 501 nm and 862 nm. The AOD at 450 nm is determined by interpolation using the Ångstrom-relation (Ångstrom, 1964). The spectral dependence of the AOD, expressed by the Ångstrom exponent alpha, is an indicator for aerosol size distribution and aerosol type (King et al., 1978; Eck et al., 1999).

For radiative transfer model calculations, the polRadtran solver (Evans and Stephens, 1991) in the libRadtran package (Mayer and Kylling, 2005) is applied which has recently been extended to treat polarization (Emde et al., 2010). Polradtran uses the doubling-and-adding method to solve the vector radiative transfer equation in a 1D plane-parallel atmosphere. Microphysical properties of aerosols, i.e. refractive indices, particle size distributions, mixtures of various aerosol types have been taken from the OPAC database (Hess et al., 1998). Assuming that the aerosol particles are spherical we may use Mie theory (Wiscombe, 1980) to compute the optical properties, i.e. scattering phase matrix, extinction coefficient, and SSA, which are needed as input for the radiative transfer solver. Here, three different aerosol mixtures comprising different SSA are used as the basis for modeling aerosol properties. The polarized sky radiance distribution for some OPAC mixtures has recently been described by (Emde et al., 2010).

3. Results

The camera system and sunphotometer have been in routine operation in Innsbruck, Austria since 2007. Sets of images are acquired every hour. For the summer in 2007 the setup was moved to Vienna. To investigate the effect of aerosols on polarization, only cloud-free conditions in constant albedo environment (snow-free in summer and autumn) and restricted range of solar zenith angles (SZA) between 55° and 60° are considered. These SZA are observable throughout most of the year in the above locations. For the effect of ground albedo, the restrictions were also cloud-free conditions and the same SZA range with AOD = 0.1 (±0.02) at 450 nm.

The characteristic distribution of polarized radiance is essentially determined by the scattering angle and the Rayleigh phase scattering function (Coulson, 1988). So for some interesting applications it suffices to consider only the principal plane (PP), a vertical cut of the hemisphere through the zenith and the sun containing a maximum of scattering angles. The maximum Π occurs at about 90° scattering angle roughly coinciding with a broad minimum of I. The following

investigation focuses on Π and I at 90° scattering angle in the PP, denoted Π_{90} and I_{90}, where the effect of AOD and albedo is close to maximal (see e.g. the sensitivity study by Boesche et al. (2006)). The angle of polarization in the PP is constant at 90°. With this constraint, measurements at two polarizer angles of 0° and 90° would suffice and the other two measurements can be used to reduce the statistical error, i.e. $I = 0.5 \times (R_0 + R_{90} + R_{45} + R_{135})$.

So for cloud-free conditions at a fixed SZA and wavelength, Π_{90} and I_{90} are functions depending on AOD and albedo which is illustrated in Fig. 1. In the calculations the AOD of an OPAC continental average aerosol mixture is scaled. The presented data will explore this dependency along the arrows in the figure.

First, Π_{90} and I_{90} for 450 nm and SZA between 55° and 60° at a constant albedo of 0.1 (snow-free environment) are plotted against the AOD in Fig. 2. For comparison, model calculations for different OPAC aerosol mixtures of continental average, urban and desert type are shown. Since no absolute calibration was performed the relative radiance was normalized to the model value (continental average aerosols) at AOD = 0.1.

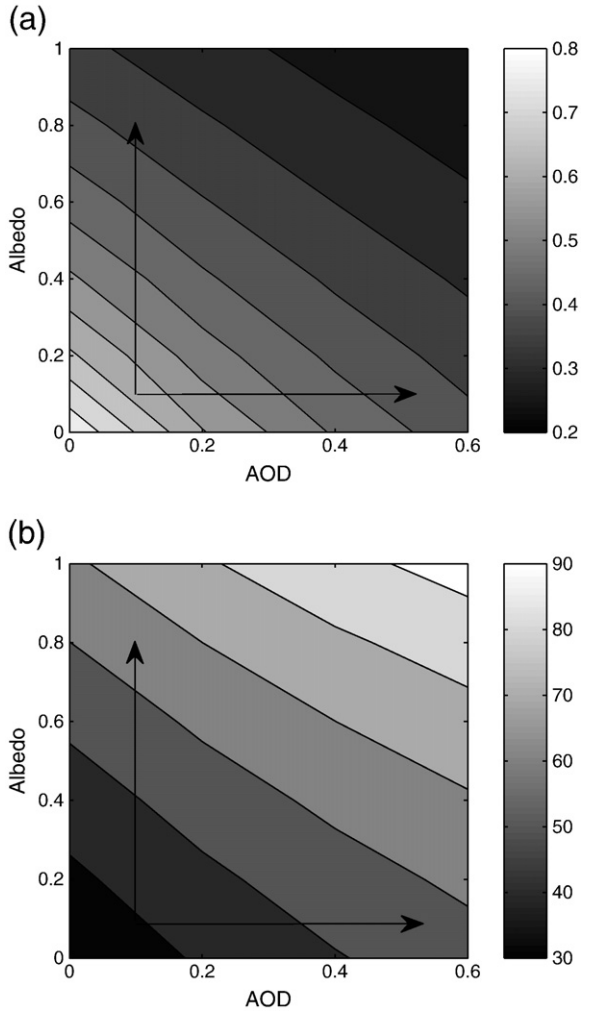

Fig. 1. a) modeled degree of polarization at 90° scattering angle in the principal plane for a continental average OPAC aerosol mixture as function of AOD and albedo at 450 nm and SZA of 60°. b) modeled sky radiance [$mW/m^2/sr/nm$] for the same parameters. The arrows indicate the range of AOD and albedo covered by the data shown in the next figures.

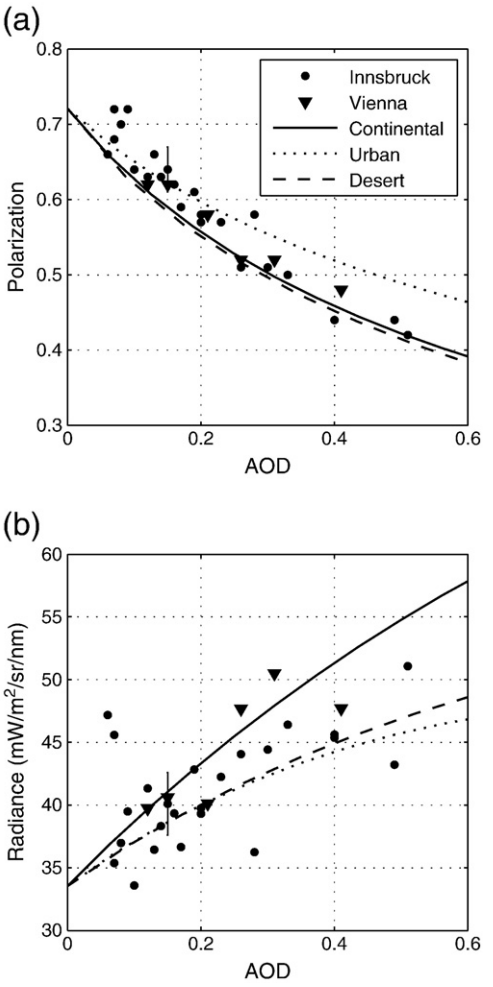

Fig. 2. a) Measured and modeled maximum degree of polarization (Π_{90}) at 450 nm in the principal plane in Innsbruck and Vienna, Austria for SZA between 55° and 60° and albedo 0.1 as function of AOD for cloud-free conditions. b) corresponding measured and modeled sky radiance. The statistical errors are indicated for a representative data point.

In the range of AODs between 0.1 and 0.5, Π_{90} is significantly reduced from 0.7 to almost 0.4. The measured radiances generally increase with higher AOD. The relatively high statistical variation partly arises from the remaining SZA-dependence of the radiance and a higher uncertainty of the radiance measurement due to minor contaminations of the camera's glass dome and reflections within the lens system. It is planned that the latter imperfections are screened for by a smoothness criterion on the complete polarization map.

Second, Π_{90} and I_{90} at a constant AOD of 0.1 under varying albedo environments are plotted (Fig. 3). Data points at effective albedo 0.1 and 0.3 were measured in Innsbruck in snow-free and partly snow-covered conditions, respectively. The data point at effective albedo 0.45 was measured at the coastline of Svalbard near Ny-Ålesund on the transition of

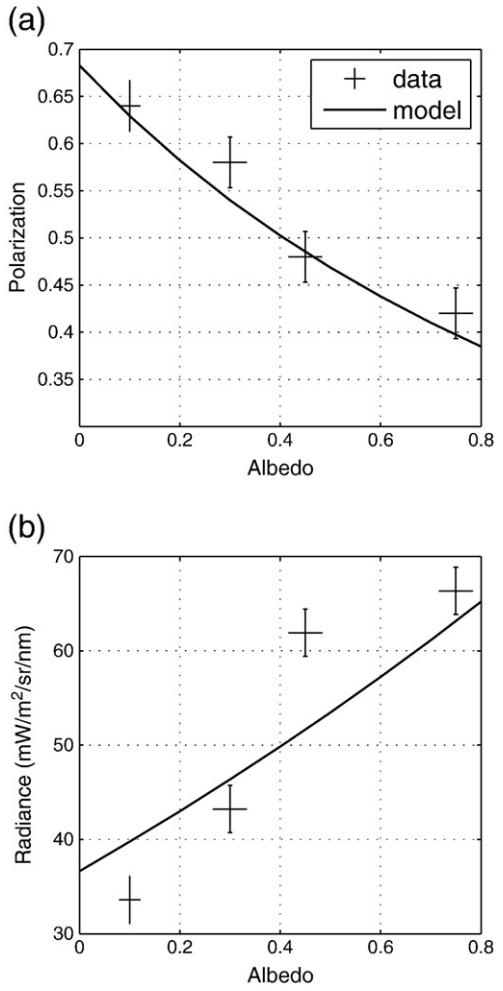

Fig. 3. a) measured and modeled maximum degree of polarization (Π_{90}) at 450 nm in the principal plane for SZA between 55° and 60° and AOD of 0.1 under different albedo environments. b) corresponding measured and modeled sky radiance.

snow and water. The effective albedo is the 1D parameter that captures the radiative influence of an inhomogeneous albedo situation. In a homogeneously snow-covered environment on Svalbard the albedo was estimated 0.75. All albedo values were derived from simultaneous global (upward looking) UV-radiation spectral measurements in comparison with libRadtran model calculations Weihs et al. (2001). All (x−) errorbars of the albedo have been estimated to be ±0.05.

4. Discussion

Measured polarizations and radiances, Π_{90} and I_{90}, as function of AOD are in the range of polRadtran model calculations considering OPAC aerosol mixtures of continental, urban and desert. The sensitivity to different aerosol mixtures increases with AOD. At AOD = 0.2, modeled Π_{90} and I_{90} vary by about 8% relatively for the modeled OPAC mixtures. The SSA for these mixtures are 0.91, 0.78 and 0.85, respectively, covering the limits of commonly encountered values. The data shown here are accumulated over 3 years and different locations, and the aerosol type is, of course, not constant. While an average continental aerosol type may be representative for typical summer days in Innsbruck (observed average Ångstrom alpha coefficient was 1.3), the data points at AOD>0.4 were taken during Saharan dust events, confirmed by a low alpha around one. Also, aerosol properties might deviate from those represented by OPAC mixtures assuming spherical particles only (Mishchenko and Travis, 1994). Specifically, dust particles usually are non-spherical and can also have a large variation of the refraction index depending on their origin.

Regarding the dependence on ground albedo, the measured polarizations agree well with the model calculations with OPAC continental average aerosols. At AOD = 0.1 the effect of the aerosol type is negligible and only the model results for the OPAC continental average are shown. The reduced Π_{90} (of 0.42) at the high albedo of 0.75 compares well with the value of 0.40 measured on Antarctica under similar conditions by Beaglehole and Carter (1992). The relatively high value of I_{90} at albedo 0.45 might be an effect of the inhomogeneous environment.

Note that all-sky polarized radiance maps contain the maximum radiative information from the sky: The three-dimensional Stokes vector as opposed to the scalar radiance, and all zenith and azimuth scattering angles, theoretically allowing any geometrical cut to be used for inversion of aerosol scattering parameters. Only the spectral information is limited for the camera used here.

Finally, it is emphasized that similarly to surface reflections, reflections from scattered clouds effects the polarized sky radiances, which must be considered when retrieving aerosol properties. It is one of the advantages of all-sky imaging that cloud information is easily retrievable from the images.

5. Conclusions

The quantitative dependence of degree of polarization and radiance at 450 nm and 90° scattering angle in the PP has been measured for a large range of AOD and albedo and is in agreement with radiative transfer calculations considering OPAC aerosol mixtures. Future improvements include reduction of the measurement statistical error and absolute radiometric calibration. Images at a series of exposure times increase the dynamic range which would allow accessing the aureole closer to the sun comprising the forward scattering angles. Eventually, the use of these three-dimensional Stokes-maps for all color channels should make an improved retrieval of aerosol scattering properties feasible.

Acknowledgements

This work was supported by the Austrian Science Fund (FWF) project P18780 and the FFG OMI project 813925. The measurements on Svalbard were supported by ARCFAC, project ID32.

References

Ångstrom, A., 1964. The parameters of atmospheric turbidity. Tellus 16, 64–75.

Beaglehole, D., Carter, G.G., 1992. Antarctic skies 2. Characterization of the intensity and polarization of skylight in a high albedo environment. J. Geophys. Res. 97 (D2), 2597–2600.
Blumthaler, M., Schallhart, B., Schwarzmann, M., McKenzie, R., Johnston, P., Kotkamp, M., Shiona, H., 2008. Spectral UV measurements of global irradiance, solar radiance, and actinic flux in New Zealand: intercomparison between instruments and model calculations. J. Atmos. Ocean. Technol. 25, 945958.
Boesche, E., Stammes, P., Ruhtz, T., Preusker, R., Fischer, J., 2006. Effect of aerosol microphysical properties on polarization of skylight: sensitivity study and measurements. Appl. Opt. 45, 8790–8805.
Chandrasekhar, S., Elbert, D., 1951. Nature 167, 51–55.
Coulson, K.L., 1988. Polarization and intensity of light in the atmosphere. Deepak, Hampton.
Coulson, K.L., Dave, J.V., Sekera, Z., 1960. Tables related to radiation emerging from a planetary atmosphere with rayleigh scattering. University of California Press, Berkeley.
Deuze, J.L., Breon, F.M., Devaux, C., Goloub, P., Herman, M., Lafrance, B., Maignan, F., Marchand, A., Nadal, F., Perry, G., Tanre, D., 2001. Remote sensing of aerosols over land surfaces from POLDER-ADEOS-1. J. Geophys. Res. 106, 4913–4926.
Dubovik, O., King, M.D., 2000. A flexible inversion algorithm for retrieval of aerosol optical properties from sun and sky radiance measurements. J. Geophys. Res. 105, 20,673–20,696.
Eck, T.F., Holben, B.N., Reid, J.S., Dubovnik, O., Smirnov, A., O'Neill, N.T., Slusker, I., Kinne, S., 1999. Wavelength dependence of the optical depth of biomass burning, urban, and desert dust aerosols. J. Geophys. Res. 104, 31,333–31,349.
Emde, C., Buras, R., Mayer, B., Blumthaler, M., 2010. The impact of aerosols on polarized sky radiance: model development, validation and applications. Atmos. Chem. Phys. 10, 383–396.
Evans, K.F., Stephens, G.L., 1991. A new polarized atmospheric radiative transfer model. J. Quant. Spectrosc. Radiat. Transfer 46 (5), 413–423.
Gál, J., Horváth, G., Meyer-Rochow, V.B., Wehner, R., 2001. Polarization patterns of the summer sky and its neutral points measured by full-sky imaging polarimetry in Finnish Lapland north of the Arctic Circle. Proc. R. Soc. Lond. A 457, 1385–1399.
Hess, M., Koepke, P., Schult, I., 1998. Optical properties of aerosols and clouds: the software package OPAC. Bull. Am. Meteorol. Soc. 79, 831–844.
Holben, B.N., Eck, T.F., Slutsker, I., Tanre, D., Buis, J.P., Setzer, A., Vermote, E., Reagan, J.A., Kaufman, Y., Nakajima, T., Lavenu, F., Jankowiak, I., Smirnov, A., 1998. AERONET— A federated instrument network and data archive for aerosol characterization. Remote Sens. Environ. 66, 1–16.
IPCC: Climate Change, 2007. 2007. Tech. Rep., Intergovernmental Panel of global climate change.
King, M.D., Byrne, D.M., Herman, B.M., Reagan, J.A., 1978. Aerosol size distribution obtained by inversion of spectral optical depth measurements. J. Atmos. Sci. 35, 2153–2167.
Kreuter, A., Zangerl, M., Schwarzmann, M., Blumthaler, M., 2009. All-sky imaging: a simple and versatile system for atmospheric research. Appl. Opt. 48 (6), 1091–1097.
Li, Z., Goloub, P., Devaux, C., Gu, X., Deuze, J.L., Qiao, Y., Zhao, F., 2006. Retrieval of aerosol optical and physical properties from ground-based spectral, multi-angular, and polarized sun-photometer measurements. Remote Sens. Environ. 101, 519–533.
Li, Z., Goloub, P., Dubovik, O., Blarel, L., Zhang, W., Andvin, T., Sinyuk, A., Sorokin, M., Chen, H., Holben, B., Tanré, D., Canini, M., Buis, J.-P., 2009. Improvements for ground-based remote sensing of atmospheric aerosol properties by additional polarimetric measurements. J. Quant. Spectrosc. Radiat. Transf. 110, 1954–1961.
Liu, Y., Voss, K., 1997. Polarized radiance distribution measurements of skylight II: experiment and data. Appl. Opt. 36, 8753–8764.
Masuda, K., Sasaki, M., Takashima, T., Ishida, H., 1999. Use of polarimetric measurements of the sky over the ocean for spectral optical thickness retrievals. J. Atmos. Ocean. Technol. 16, 856–859.
Mayer, B., Kylling, A., 2005. Technical note: the libRadtran software package for radiative transfer calculations — description and examples of use. Atmos. Chem. Phys. 5, 1855–1877.
Mishchenko, M.I., Travis, L.D., 1994. Light scattering by polydispersions of randomly orientated spheroids with sizes comparable to wavelengths of observation. Appl. Opt. 33 (30), 7206–7225.
Mishchenko, M.I., Cairns, B., Kopp, G., Schueler, C.F., Fafaul, B.A., Hansen, J.E., Hooker, R.J., Itchkawich, T., Maring, H.B., Travis, L.D., 2007. Accurate monitoring of terrestrial aerosols and total solar irradiance: introducing the Glory Mission. Bull. Am. Meteorol. Soc. 88, 677–691.
North, J.A., Duggin, M.J., 1997. Stokes vector imaging of the polarized sky-dome. Appl. Opt. 36, 723–730.
Shukurov, A.K., Shukurov, K.A., 2006. Field studies of the correlation between the atmospheric aerosol content and the light polarization at the zenith of the daytime sky. Izv. Atmos. Ocean. Phys. 42, 68–73.
Vermeulen, A., Devaux, C., Herman, M., 2000. Retrieval of the scattering and microphysical properties of aerosols from ground-based optical measurements including polarization. I. method. Appl. Opt. 39, 6207–6220.
Weihs, P., Lenoble, J., Blumthaler, M., Martin, T., Seckmeyer, G., Philipona, R., la Casiniere, A.D., Sergent, C., Gröbner, J., Cabot, T., Masserot, D., Pichler, T., Pougatch, E., Rengarajan, G., Schmucki, D., Simic, S., 2001. Modeling the effect of an inhomogeneous surface albedo on incident UV radiation in mountainous terrain: determination of an effective surface albedo. Geophys. Res. Lett. 28, 3111–3114.
Wiscombe, W.J., 1980. Improved mie scattering algorithms. Appl. Opt. 19, 1505–1509.